Diagn Interv Radiol 2020; 26:411–419

© Turkish Society of Radiology 2020

ABDOMINAL IMAGING

ORIGINAL ARTICLE

# Radiomics-based nomogram using CT imaging for noninvasive preoperative prediction of early recurrence in patients with hepatocellular carcinoma

Hong-Bo Zhu
Ze-Yu Zheng
Heng Zhao
Jing Zhang
Hong Zhu
Yue-Hua Li
Zhong-Yi Dong
Lu-Shan Xiao
Jun-Jie Kuang
Xiao-Li Zhang
Li Liu

**PURPOSE**
The aim of this study was to develop and validate a radiomics nomogram based on radiomics features and clinical data for the noninvasive preoperative prediction of early recurrence (≤2 years) in patients with hepatocellular carcinoma (HCC).

**METHODS**
We enrolled 262 HCC patients who underwent preoperative contrast-enhanced computed tomography (CT) and curative resection (training cohort, n=214; validation cohort, n=48). We applied propensity score matching (PSM) to eliminate redundancy between clinical characteristics and image features, and the least absolute shrinkage and selection operator (LASSO) was used to prevent overfitting. Next, a radiomics signature, clinical nomogram, and combined clinical-radiomics nomogram were built to predict early recurrence, and we compared the performance and generalization of these models.

**RESULTS**
The radiomics signature stratified patients into low-risk and high-risk, which showed significant difference in recurrence-free survival and overall survival ($P \leq 0.01$). Multivariable analysis identified dichotomized radiomics signature, alpha-fetoprotein, and tumor number and size as key early recurrence indicators, which were incorporated into clinical and radiomics nomograms. The radiomics nomogram showed the highest area under the receiver operating characteristic curve (AUC), with significantly superior predictive performance over the clinical nomogram in the training cohort (0.800 vs. 0.716, respectively; $P = 0.001$) and the validation cohort (0.785 vs. 0.654, respectively; $P = 0.039$).

**CONCLUSION**
The radiomics nomogram is a noninvasive preoperative biomarker for predicting early recurrence in patients with HCC. This model may be of clinical utility for guiding surveillance follow-ups and identifying optimal interventional strategies.

Hepatocellular carcinoma (HCC) has a high prevalence and mortality (1). One of the principal challenges in overcoming the poor prognosis of patients with HCC is the high recurrence rate after curative resection (2, 3). Although patients with early stage HCC are candidates for potentially curative resection with a 50%–70% 5-year survival rate (2), resection is also associated with a high rate of recurrence and accounts for 70% of tumor recurrence cases at 5 years post resection (2, 3). Tumor recurrence is divided into true recurrence (intrahepatic metastases) and *de novo* tumors within the oncogenic liver (2–5). Additionally, although robust clinical definitions of these entities have not been established, a cutoff of 2 years has been adopted for gross classification of early and late recurrences (2, 3, 6). Tumor recurrence is the main reason for the reduced survival of HCC patients. Specifically, early tumor recurrence related to intrahepatic metastases results in a 24% decrease in the 5-year survival and a 54-month decrease in the median survival of HCC patients (2, 3, 5). Therefore, precise preoperative screening is necessary to facilitate effective and personalized preventive strategies for these patients. Some studies have identified several risk factors that account for early recurrence, including high serum alpha-fetoprotein (AFP) level, large tumor size, the presence of venous invasion, tumor rupture, and antiviral therapy, but controversy still exists as to which

From the Department of Infectious Diseases (H.B.Z., L.S.X., L.L. ✉ *18602062738@163.com*), Nanfang Hospital, Southern Medical University, Guangzhou, China; Departments of Oncology (H.B.Z., Y.H.L.), Radiology (H.Zhao), Pathology (X.L.Z.), the First Affiliated Hospital of University of South China, Hengyang, China; Departments of Medical Imaging Center (Z.Y.Z., J.Z.), Oncology (Z.Y.D., J.J.K.), and Management and Big Data Center (H.Zhu), Nanfang Hospital, Southern Medical University, Guangzhou, China.

Received 04 December 2019; revision requested 05 January 2020; last revision received 09 March 2020; accepted 19 March 2020.

Published online 03 June 2020.

DOI 10.5152/dir.2020.19623

You may cite this article as: Zhu HB, Zheng ZY, Zhao H, et al. Radiomics-based nomogram using CT imaging for noninvasive preoperative prediction of early recurrence in patients with hepatocellular carcinoma. Diagn Interv Radiol 2020; 26:411–419

of these risk factors are more important for recurrence (7–9). Aided by advances in biological and genomic technologies, many studies have developed predictive and prognostic molecular signatures for HCC (10), but these signatures often rely on post-operative and invasive features, such as microvascular invasion and genomic analysis. In addition, as tumors are spatially and temporally heterogeneous, general gene-expression profiles determined from small portions of tumor tissue do not allow for a real-time and complete characterization of the pathophysiology of the tumor (4, 11).

Radiomics is an emerging methodology combining key features into an image-based biomarker for monitoring, diagnosis, prognosis, and prediction in medical research, and is considered to bridge the gap between medical imaging and personalized medicine (12, 13). Radiomics can capture the three-dimensional information of the total tumor and has proved effective in characterizing the heterogeneity of the tumor by acting as a whole tumor virtual biopsy (12, 14). A few radiomics analyses based on contrast-enhanced computed tomography (CT) and magnetic resonance imaging (MRI) have been conducted to predict the recurrence of HCC (15–26). However, these studies had some inherent limitations: for example, these studies did not include validation cohorts, the quantifying imaging features were extracted from the largest cross-section of the tumor, and subjectively determined features were used to build the models. In addition, few studies have compared the predictive performance of radiomics and clinical models and evaluated the potential improvement in predictive capacity of radiomics over clinical models. Furthermore, imaging features have been proven to capture tumor heterogeneity and can also be used to reconstruct the genomic characteristics of highly heterogeneous cancers (14, 27, 28). While more radiomics models are being developed, the interpretability and credibility of the models are very poor due to the difficulty in understanding the radiomics features.

Therefore, the purpose of this study was to develop and validate radiomics models based on contrast-enhanced CT for the preoperative prediction of early recurrence and prognosis of patients with HCC. Further, we explored the complementary relationship between the radiomics model with a readily accessible clinical model.

**Main points**

- The radiomic signature based on contrast-enhanced CT was able to stratify HCC patients into low-risk and high-risk groups, which differed in recurrence-free survival and overall survival.
- The radiomic nomogram, which integrates a dichotomised radiomic signature as well as clinical characteristics, has better predictive performance than the clinical nomogram alone, for predicting early recurrence of HCC.
- Radiomic nomogram is useful for noninvasively identifying HCC patients with high early recurrence risk after curative resection.

## Methods

### Patients

This retrospective study included consecutive patients with HCC who underwent resection with curative intent at the Nanfang Hospital, Southern Medical University (NFHSMU) (years of curative resection 2014–2017) or the First Affiliated Hospital of University of South China (FAHUSC) (2014–2017) or who were included in the database of the cancer imaging archive (TCIA) and the cancer genome atlas (TCGA). The flowchart detailing the inclusion and exclusion criteria is presented in Supplementary S1 and Fig. S1.

This study was approved by our institutional review board (NFEC-201208-K3) and complied with the Declaration of Helsinki. Informed consent was waived for this retrospective research. The overall workflow is presented in Fig. 1.

### Follow-up

Patients were required to attend a follow-up appointment 1 month after the surgery. A second follow-up appointment was required at 3–4 months, and every 4–6 months thereafter (2). Any new lesions confirmed by contrast-enhanced CT, contrast-enhanced MRI, or histopathology were accepted as recurrence. Recurrence-free survival (RFS) was defined as the time from the date of resection to the date of recurrence, metastasis, last follow-up, or death from any cause. Overall survival (OS) was defined as the time from the date of resection to death from any cause or to the last follow-up. Patients were censored in cases of no recurrence by 2 years or on 1 July 2019 (whichever came first). The follow-up plan for TCGA and TCIA was as reported previously (29).

### CT image acquisition, segmentation, pre-processing and extraction of radiomics features

Supplementary S2 describes CT image acquisition, the image operation process, and the image segmentation. Radiomics features were extracted from each volume-of-interest (VOI) using the pyradiomics package (http://www.radiomics.io/pyradiomics.html; version 2.2.0; Computational Imaging and Bioinformatics Lab, Harvard Medical School). The pyradiomics package was run in Python (https://www.python.org/; version 3.7; open source software; Python Software Foundation). Supplement S2 also describes intraobserver (reader 1 twice) and interobserver (reader 1 vs. reader 2) reproducibility evaluation. In patients with multiple (two or more) lesions, the largest lesion was segmented and used for subsequent analysis. Intraclass correlation coefficient (ICC) >0.75 indicates a good agreement (30). The categories of imaging features and primary filtering process are detailed in Supplementary S3 and S4.

### Feature selection and radiomics model building

We conducted statistical tests for baseline clinical characteristics in patients with and without early recurrence and found that AFP, tumor number, and tumor size were significantly different between the two groups in the training cohort. In order to select effective and complementary imaging features that were independent of these aforementioned clinical variables, we applied propensity score matching (PSM) to achieve a balance between the two groups in the training cohort (Supplementary S4; Fig. S2). The least absolute shrinkage and selection operator (LASSO) on the logistic regression model was used to select variables for constructing a prediction model. Then, the predictive model was validated in the validation cohort. Furthermore, we applied the Youden index to determine the optimal cutoff value for dichotomizing the radiomics scores and stratifying patients according to their risk of early recurrence (i.e., low- and high-risk of early recurrence).

### Construction and validation of the radiomics-based nomogram

Multivariable logistic regression analysis was applied to test the independent significance of different factors on tumor recurrence (the *P* value threshold was set to

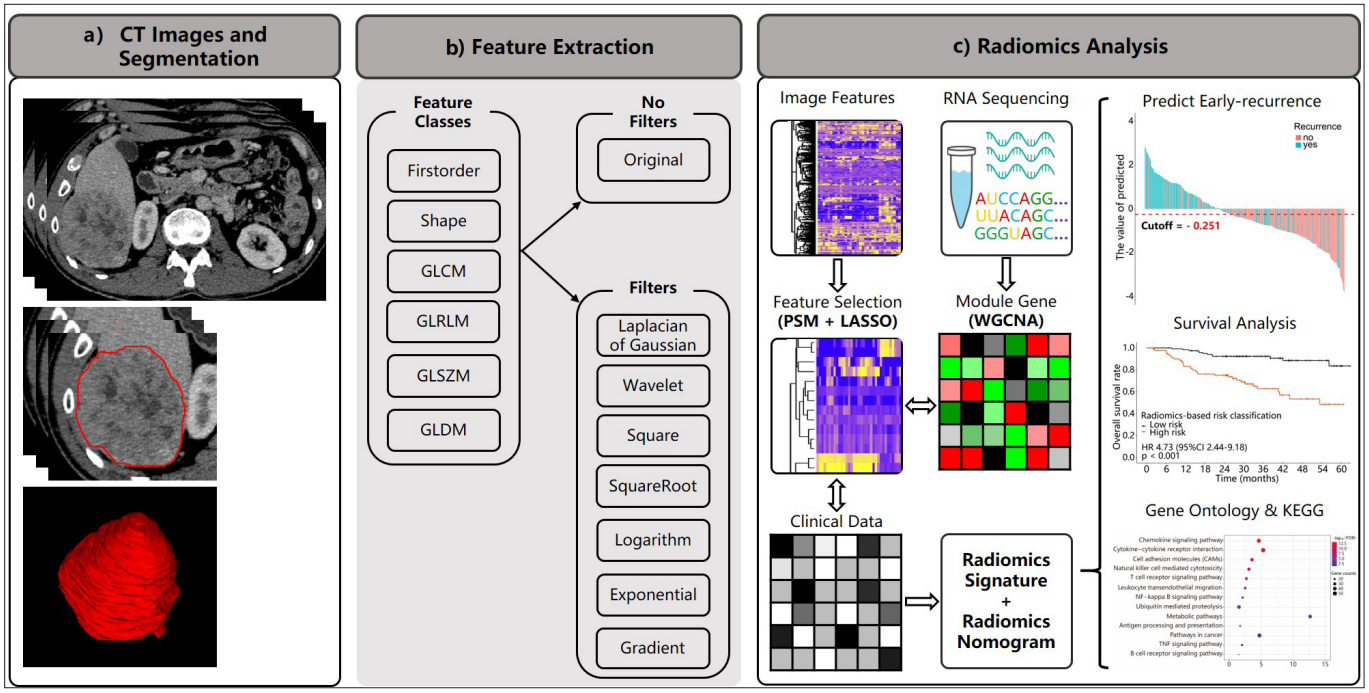



**Figure 1. a–c.** The workflow of the current study. In panel **(a)**, we obtained venous-phase contrast-enhanced CT images and segmented the volume of interest; panel **(b)** shows categories of extracted features; panel **(c)** shows the workflow outlining the process of features extraction and selection, of radiomics signatures and radiomics nomogram building, clinical utility assessment of the model (prediction of early recurrence and survival risk stratification), an exploratory analysis of small sample to construct the gene module with weighted gene co-expression network analysis (WGCNA), and the association between the predictive value of radiomics features and gene pathways using gene ontology and the Kyoto Encyclopedia of Genes and Genomes (KEGG) databases.

$P < 0.15$). Candidate predictors included dichotomized radiomics signature, AFP, tumor number, and tumor size. We constructed two nomograms, with or without dichotomized radiomics signature, to explore improvement in the predictive performance of the radiomics nomogram, as compared with clinical parameters. The area under the receiver-operating characteristic (ROC) curve (AUC) was utilized to illustrate the predictive performance, and the Delong test was applied to determine whether the difference was significant. Calibration curves were assessed graphically by plotting the observed rates against the nomogram-predicted probabilities. A Hosmer–Lemeshow test was used to assess the uniformity between the observed and predicted values.

### Statistical analysis

All statistical analyses were conducted using R software (http://www.Rproject.org; version 3.5.2; open source software, The R Foundation) and SPSS software (version 22.0; IBM Corp.). Continuous variables were compared between groups using the independent samples t-test for variables with a normal distribution or the Mann-Whitney U test for variables with an abnormal or unknown distribution. Categorical variables were compared between groups using the chi-square test or Fisher's test where appropriate. The association of variables with early recurrence was assessed using logistic regression analysis. The "pROC" package was used to plot the ROCs and measure the AUC. Survival curves were generated using the Kaplan-Meier method and compared using a two-sided log-rank test. The other R software packages used for statistical analysis and plotting were listed in Supplementary S5. A two-sided $P$ value of <0.05 was considered statistically significant.

## Results

Overall, 262 HCC patients were included in the current study. Of these, 119 patients were diagnosed with early recurrence (93 in the training cohort and 26 in the validation cohort); the baseline characteristics of patients in the training and validation cohorts are presented in the Table. Patients with early recurrence had higher AFP levels, more tumors, and larger tumors than did patients without early recurrence in the training cohort.

In total, 1665 features were extracted from the VOIs in portal venous phase contrast-enhanced CT images. After the reproducibility analysis, we derived 1497 and 1532 common features with inter- and intraobserver ICC >0.75, separately. Then, the 1475 common features that were reproducible in both intra- and interobserver analysis were adopted for subsequent analysis. The heatmap demonstrated that early recurrence, AFP levels, BCLC stage, tumor number, and tumor size were consistently differentially distributed in these clusters (Fig. 2). As the baseline clinical characteristics in the groups with and without early recurrence were not balanced (Table), we matched 70 pairs of cases for all risk factors using a PSM analysis and selected features that were not redundant with the clinical characteristics and that differed significantly between the two groups. The relative multivariate imbalance L1 before the PSM is 0.345, and the value change to 0.043 after PSM, which means that we get a balance of covariate between the early recurrence group and no early recurrence group. The 1475 features were thus converged to 59 potential predictors in the training cohort after PSM, based on the outcomes of univariate logistic regression analysis with a threshold $P = 0.15$.

The putative predictive imaging features were entered into the LASSO logistic regression model. With 10-fold cross-validation, filtered no-overfitting features were used to construct the radiomics signature with the maximal AUC in the total training cohort

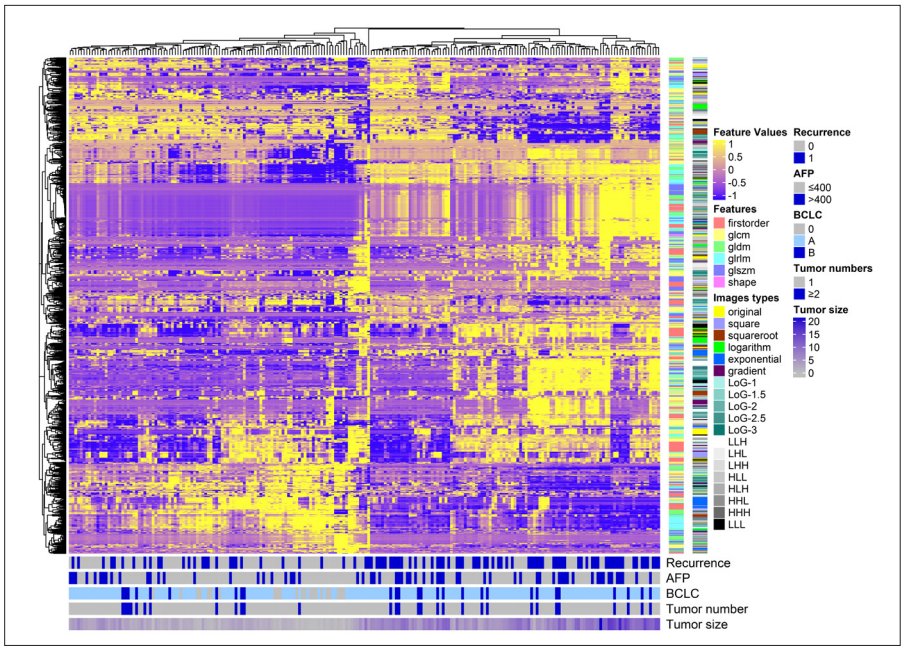



**Figure 2.** Radiomics heatmap. Unsupervised clustering of patients with hepatocellular carcinoma in the training cohort (y-axis) and radiomics feature expression (n=1475; x-axis) revealed clusters of patients with similar radiomics expression characteristics. AFP, serum alpha-fetoprotein; BCLC, Barcelona clinical liver cancer staging.

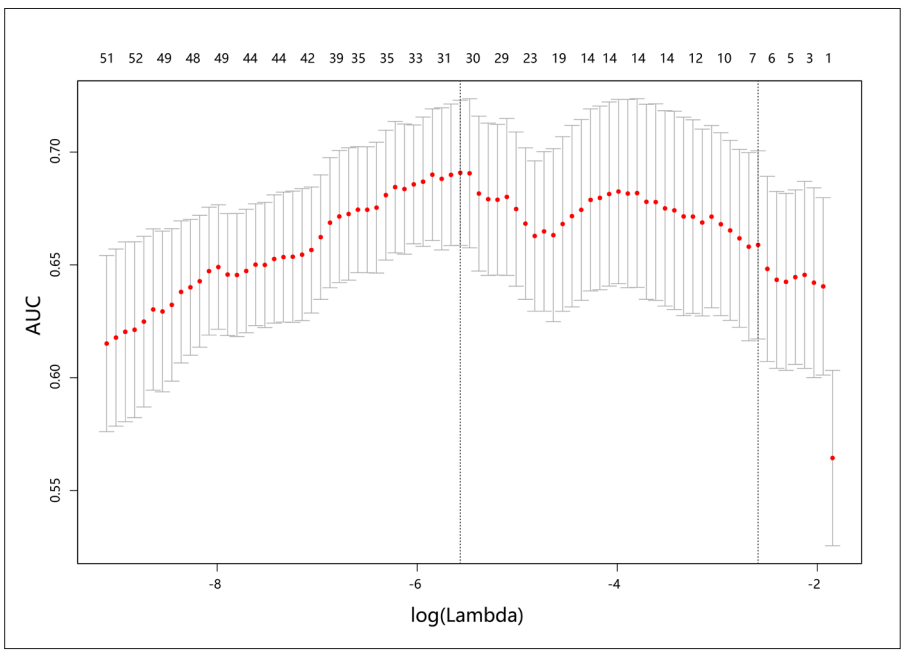



**Figure 3.** Selection of radiomics features using the least absolute shrinkage and selection operator (LASSO) binary logistic regression. Turning parameter (λ) selection in the LASSO model used a 10-fold cross-validation via minimum criteria, and optimal λ resulted in 30 nonzero coefficients. The area under the receiver operating characteristic (AUC) curve was plotted versus log (λ). Dotted vertical lines were drawn at the optimal values by using the minimum criteria and 1 standard error of the minimum criteria (the 1-SE criteria) according to 10-fold cross-validation. The minimum criteria were chosen as the optimal λ with the largest AUC in the training data set, which resulted in 30 non-zero coefficients.

(Fig. 3). A risk score was calculated for each patient using the formula derived from the expression value of these features, weighted by their regression coefficient (Supplementary S6). The radiomics scores of patients with early recurrence were generally higher than those of patients without early recurrence in the training cohort (0.41 vs. -0.94; $P < 0.001$). This finding was also confirmed in the validation cohort (0.36 vs. -0.88; $P = 0.008$) (Table).

On the basis of the maximum Youden index, we used an AUC to determine the optimal cutoff value (-0.251) based on the training cohort data. The optimal cutoff value was applied to the training and validation cohorts to separate patients into low-risk and high-risk groups (Fig. 4a, Fig. S3). This dichotomized radiomics signature yielded an AUC of 0.749 in the training cohort (95% CI, 0.690 to 0.808; $P < 0.001$) and an AUC of 0.759 in the validation cohort (95% CI, 0.640 to 0.877; $P < 0.001$) (Fig. 4b, 4c).

In the training cohort, patients belonging to the high-risk group had shorter RFS (hazard ratio [HR] 4.650; 95% CI, 3.080 to 7.030, $P < 0.001$) and shorter OS (HR 4.73; 95% CI, 2.440 to 9.180, $P < 0.001$) (Fig. 4d, 4e). Similarly, in the validation cohort, patients belonging to the high-risk group had shorter RFS (HR 2.820; 95% CI, 1.320 to 6.020; $P < 0.001$) and OS (HR 4.420; 95% CI, 1.290 to 15.130; $P = 0.010$) (Fig. 4f, 4g).

By applying multivariate logistic regression analysis, we identified that the dichotomized radiomics signature, AFP level, tumor number, and tumor size were the key parameters related to early recurrence in patients with HCC (Supplementary S7). Among these factors, the dichotomized radiomics signature had the highest odds ratio (OR 6.399; 95% CI, 3.219 to 12.723; $P < 0.001$). Next, we developed two nomograms that incorporated the above independent predictors: 1) the radiomics nomogram, which comprised the dichotomized radiomics signature along with clinical risk factors, and 2) the clinical nomogram, which included only clinical risk factors (Fig. 5a; Fig. S4). Our results demonstrated that the predictive performance of the radiomics nomogram was significantly better than that of the clinical nomogram (AUC 0.800; 95% CI, 0.740 to 0.859 vs. AUC 0.716; 95% CI, 0.690 to 0.808; $P < 0.001$ in the training cohort and AUC 0.785; 95% CI, 0.657 to 0.913 vs. AUC 0.654; 95% CI, 0.505 to 0.803; $P = 0.039$ in the validation cohort). The calibration curve of the radiomics nomogram demonstrated that there was a strong agreement between the prediction of early recurrence and the actual observation of early recurrence in the training cohort and in the validation cohort (Fig. 5b, 5c). The Hosmer-Lemeshow test revealed that there were no significant differences between the predictive calibration curve and the ideal calibration curve for the prediction of early

**Table.** Baseline characteristics of patients

| Variable | Training cohort | | *P* | Testing cohort | | *P* |
|---|---|---|---|---|---|---|
| | No-early recurrence (n=121) | Early recurrence (n=93) | | No-early recurrence (n=22) | Early recurrence (n=26) | |
| Age (years), mean±SD | 50.8±12.7 | 50.7±11.8 | 0.967 | 53.8±9.1 | 58.5±12.7 | 0.082 |
| Sex, n (%) | | | | | | |
| Female | 15 (12.4) | 11 (11.8) | 0.900 | 2 (9.0) | 8 (30.8) | 0.137 |
| Male | 106 (87.6) | 82 (88.2) | | 20 (90.9) | 18 (69.2) | |
| Hepatitis B, n (%) | | | | | | |
| Negative | 10 (8.3) | 7 (7.5) | 0.843 | 6 (27.3) | 13 (50.0) | 0.109 |
| Positive | 111 (91.7) | 86 (92.5) | | 16 (72.7) | 13 (50.0) | |
| Hepatitis C, n (%) | | | | | | |
| Negative | 121 (100.0) | 92 (98.9) | 0.435 | 22 (100.0) | 23 (88.5) | 0.295 |
| Positive | 0 (0.0) | 1 (1.1) | | 0 (0.0) | 3 (11.5) | |
| Child-Pugh, n (%) | | | | | | |
| A | 117 (96.7) | 84 (90.3) | 0.053 | 22 (100.0) | 23 (88.5) | 0.295 |
| B | 4 (3.3) | 9 (9.7) | | 0 (0.0) | 3 (11.5) | |
| ALT*, n (%) | | | | | | |
| ≤40 U/L | 88 (72.7) | 66 (71.0) | 0.776 | - | - | - |
| >40 U/L | 33 (27.3) | 27 (29.0) | | | | |
| AST*, n (%) | | | | | | |
| ≤40 U/L | 115 (95.0) | 91 (97.8) | 0.478 | - | - | - |
| >40 U/L | 6 (5.0) | 2 (2.2) | | | | |
| AFP, n (%) | | | | | | |
| ≤400 ng/mL | 94 (77.7) | 56 (60.2) | 0.006 | 19 (86.4) | 22 (84.6) | 1.000 |
| >400 ng/mL | 27 (22.3) | 37 (39.8) | | 3 (13.6) | 4 (15.4) | |
| Radiologic evidence of cirrhosis*, n (%) | | | | | | |
| Absent | 53 (43.8) | 29 (31.2) | 0.060 | - | - | - |
| Present | 68 (56.2) | 64 (68.8) | | | | |
| BCLC stage, n (%) | | | | | | |
| 0 + A | 111 (90.2) | 75 (80.0) | 0.017 | 20 (91.0) | 18 (69.2) | 0.137 |
| B | 10 (9.8) | 18 (20.0) | | 2 (9.0) | 8 (30.8) | |
| Tumor number, n (%) | | | | | | |
| ≤1 | 111 (91.7) | 73 (78.5) | 0.006 | 20 (91.0) | 18 (69.2) | 0.137 |
| >1 | 10 (8.3) | 20 (21.5) | | 2 (9.0) | 8 (30.8) | |
| Tumor size, n (%) | | | | | | |
| ≤5 cm | 81 (66.9) | 33 (35.5) | <0.001 | 13 (59.1) | 10 (38.5) | 0.154 |
| >5 cm | 40 (33.1) | 60 (64.5) | | 9 (40.9) | 16 (61.5) | |
| Radiomic signature score, median (interquartile range) | -0.94 (-1.60, -0.31) | 0.41 (-0.38, 1.19) | <0.001 | -0.89 (-1.27, -0.45) | 0.36 (-0.91, 1.45) | 0.008 |

SD, standard deviation; ALT, alanine aminotransferase; AST, aspartate aminotransferase; AFP, serum alpha-fetoprotein; BCLC, Barcelona clinical liver cancer staging.
*No corresponding variables recorded in TCIA&TCGA cohort.

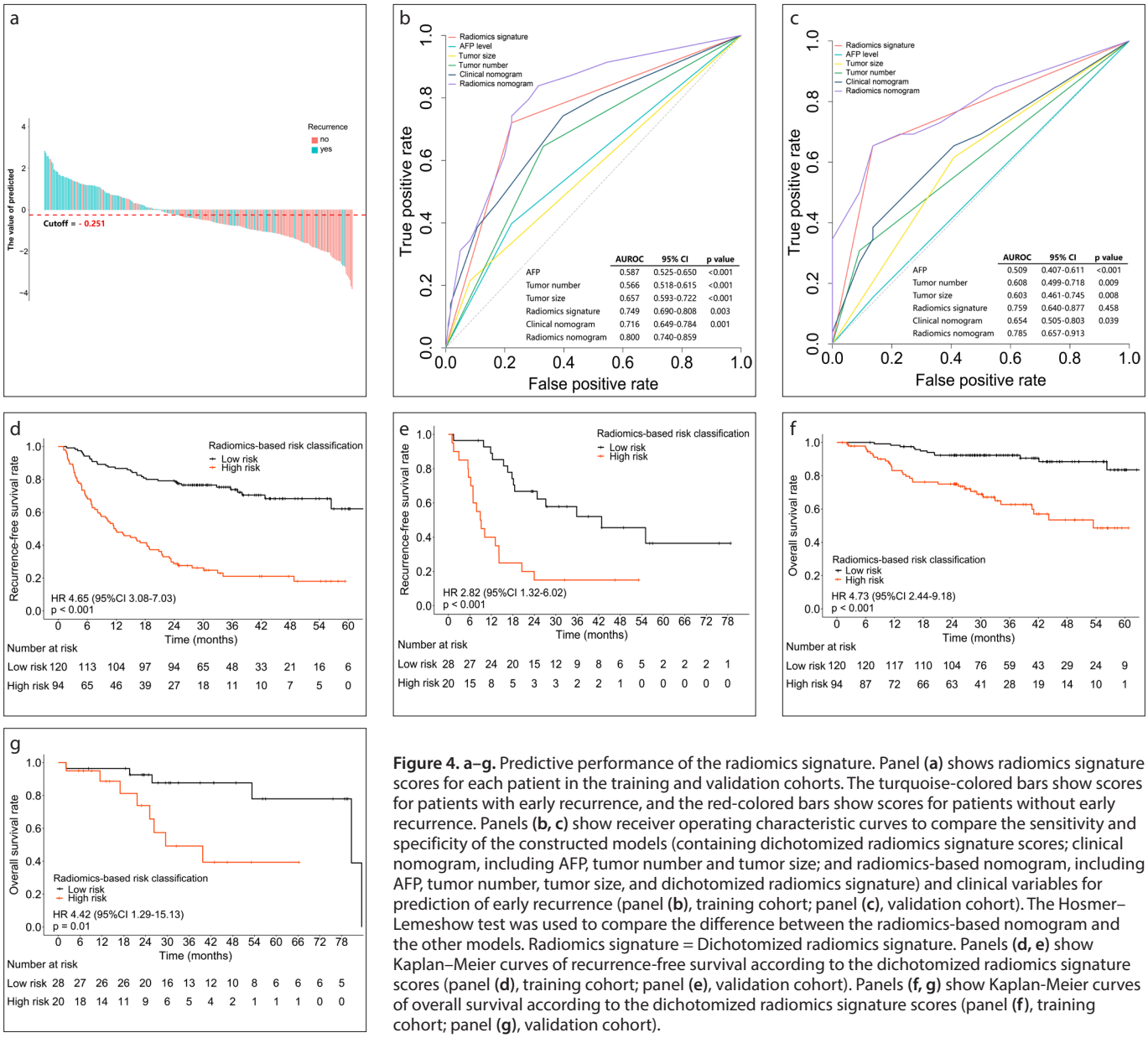



**Figure 4. a–g.** Predictive performance of the radiomics signature. Panel **(a)** shows radiomics signature scores for each patient in the training and validation cohorts. The turquoise-colored bars show scores for patients with early recurrence, and the red-colored bars show scores for patients without early recurrence. Panels **(b, c)** show receiver operating characteristic curves to compare the sensitivity and specificity of the constructed models (containing dichotomized radiomics signature scores; clinical nomogram, including AFP, tumor number and tumor size; and radiomics-based nomogram, including AFP, tumor number, tumor size, and dichotomized radiomics signature) and clinical variables for prediction of early recurrence (panel **(b)**, training cohort; panel **(c)**, validation cohort). The Hosmer–Lemeshow test was used to compare the difference between the radiomics-based nomogram and the other models. Radiomics signature = Dichotomized radiomics signature. Panels **(d, e)** show Kaplan–Meier curves of recurrence-free survival according to the dichotomized radiomics signature scores (panel **(d)**, training cohort; panel **(e)**, validation cohort). Panels **(f, g)** show Kaplan-Meier curves of overall survival according to the dichotomized radiomics signature scores (panel **(f)**, training cohort; panel **(g)**, validation cohort).

recurrence in both cohorts ($P = 0.525$ and $P = 0.780$ for the training and validation cohorts, respectively).

## Discussion

We evaluated the utility of a radiomics nomogram derived from clinical and CT data for the noninvasive preoperative and real-time prediction of early recurrence of HCC patients who underwent curative surgery. The radiomics signature was found to be effective for predicting early recurrence, and the dichotomized radiomics signature successfully stratified patients according to their risk of early recurrence and differences in RFS and OS. After we incorporated the dichotomized radiomics signature and the clinical risk factors (AFP, tumor number, and tumor size) into a convenience radiomics nomogram, the predictive performance and generalizability were further improved compared with the readily accessible clinical model. Both radiomics-based models offer clinically utility, which may help clinicians design more effective treatment strategies tailored to the specific characteristics of individual patients and their disease.

Radiomics has been recognized as an important imaging biomarker in oncology; however, some methodological and technical inconsistencies have limited its clinical application (12). For example, there is currently no validation process for developing a radiomics model (15, 16, 23, 24). In our study, the radiomics nomogram demonstrated outstanding discrimination in both training (AUC, 0.800; 95% CI, 0.740 to 0.859) and validation cohorts (AUC, 0.785; 95% CI 0.657 to 0.913). Next, considering that tumors are spatially and temporally heterogeneous, the largest cross-section of the image cannot fully capture this heterogeneity, just as the genomic data extracted from a small portion of tumor tissue does not represent the entire tumor (15, 18, 23, 24). Therefore, we delineated the whole volume of the tumor to comprehensively characterize the underlying pathophysiology.

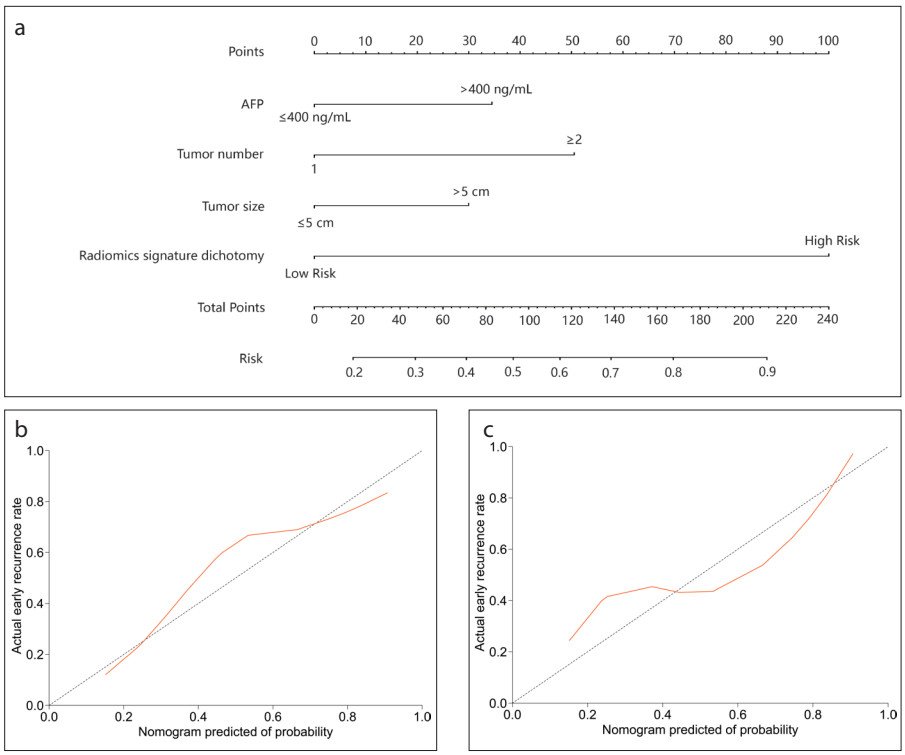



**Figure 5. a–c.** Developed nomogram and calibration curves of the nomogram. Panel **(a)** shows the nomogram developed to predict the risk of early recurrence in patients with hepatocellular carcinoma who underwent resection with curative intent (including AFP, tumor number, tumor size, and dichotomized radiomics signature). Panels **(b, c)** show the calibration curves of the radiomics-based nomogram, which was used to depict the calibration of each model in terms of the agreement between the predicted risks of early recurrence and observed outcomes of early recurrence. The y-axis represents the actual early recurrence, and the x-axis represents the predicted risk of early recurrence. The diagonal dotted line represents perfect prediction by an ideal model. The red-colored solid line represents the performance of the nomogram; a closer fit to the diagonal dotted line represents better predictive performance (panel **(b)**, training cohort; panel **(c)**, validation cohort).

Additionally, some early predictive radiomics models are based on semantic image features, which are subjective and experience-dependent (31, 32). The radiomics model presented here is based on computational image features, which are objective and highly reproducible. Furthermore, imaging features were extracted from images obtained in multiple centers that used different CT scanners, standard operating procedures for contrast-enhanced CT, slice thicknesses, voltages, and other machine parameters (12). Aerts et al. (14) suggested that the power of radiomics may be improved by using normalization methods and Sun et al. (33) noted that the peak kilovoltage, an image acquisition variable, is a significant factor in a radiomics model for predicting tumor-infiltrating CD8+ T cells, which highlights the need to consider the image acquisition parameters during modelling. A number of studies have described the details of avoiding the variability of features extracted from images (15, 16, 18, 19, 22–26). Recent CT radiomics studies have reported that using grey-level normalization and voxel-size resampling greatly reduced the differences in scanners and CT parameters (12, 34). Since the present study utilized multiple CT scanners and different parameter settings, we applied normalization and resampling to the images before feature extraction in order to standardize imaging features.

Radiomics features could represent the tumor phenotype and the tumor microenvironment, which are distinct from other pertinent data sources (including clinically obtained, treatment-related, or genomic data) (12, 14, 27, 33). Therefore, radiomics-based models should be compared with clinical characteristics in order to explore whether the combined radiomics-clinical model can improve the predictive performance of the clinical model alone. In other words, the features used to develop a predictive radiomics model were selected because they were capable of predicting early recurrence, not because they were simply significantly associated with clinical characteristics that were themselves significantly associated with early recurrence. Chan et al. (8) developed a preoperative, noninvasive model (ERASL-pre) using readily accessible clinical factors that could successfully stratify patients into three groups based on the risk of early recurrence of HCC. Kim et al. (17) revealed that their radiomics model added no additional value as compared with the clinicopathologic model. In order to develop a robust and generalized model, we should remove the overfitting issues of high dimensional imaging features. However, few studies have attempted to eliminate the redundancy between imaging features and clinical data and to select the complementary imaging features for subsequent analysis. In the present study, since there was an imbalance in the clinical data between the groups with and without early recurrence, we applied PSM to achieve balanced pairs in which to screen for independent imaging features and construct a radiomics signature that was not affected by the clinical variables. We then incorporated the dichotomized radiomics signature and clinical nomogram into a radiomics nomogram, which improved the performance of the clinical nomogram (Fig. 4b, 4c).

In the present study, 30 radiomics quantitative features were identified as most associated with early recurrence. Among them, 28 were texture features, including histogram, glcm, gldm, glrlm, and glszm, and 2 were morphological features. Among texture features, glcm, gldm, glrlm, and glszm reflect signal mixing degree of the lesions by means of relative relationship between distribution and site of the gray level, and thus important markers of intratumor heterogeneity (12, 14, 27). Although these features could reflect different aspects of textural information and the underlying tumor biology, the correlation between a single radiomics feature and the biological behavior is difficult to grasp intuitively (14). Therefore, construction of a multi-feature model is a more robust and generalized approach for outcome estimation, which can comprehensively represent the heterogeneity of the tumor. Although many studies revealed that radiomics features can capture the heterogeneity of tumors, it is not clear how the radiomics features could predict the recurrence rate of a patient who received radi-

cal hepatectomy (12, 13, 27). Therefore, it is important to inform clinicians that the radiomics features are not pixels in an image, but rather represent specific molecular biological functions that mediate the progression and metastasis of tumors. An exploratory analysis of a small sample was conducted to identify the association between the radiomics features and underlying pathophysiology. As demonstrated in Supplementary S8, we observed the radiomics features that significantly associated with gene pathways related to cell cycle progression, extracellular matrix, cell adhesion, cell chemotaxis, angiogenesis, and immune response (Fig. S5).

Considering the high rate of early recurrence in patients that received radical hepatectomy, many neoadjuvant and adjuvant schemes have been applied to reduce the risk of tumor recurrence and prolong the OS. While the effectiveness of the existing interventional method is controversial (35), it was speculated that the discrepancy in these findings may be attributed to a lack of screening out potentially high-risk patients that actually require neoadjuvant or adjuvant treatments. Therefore, an effective biomarker for identifying patients with a high risk of recurrence is urgently needed. As demonstrated in the decision curve analysis (Fig. S6), the clinical decision brought by the radiomics model may provide a net benefit by setting a threshold; for example, when a patient is identified to have a high risk of early recurrence, extra neoadjuvant or adjuvant treatment options, such as transarterial chemoembolization, transarterial radioembolization, chemoprevention, and targeted therapy, may be prescribed. Though the performance and generality of the radiomics model require more samples, multicenter, and prospective validation, it provides a new potential biomarker to identify patients with a high risk of early recurrence.

The present study has some limitations. First, this was a retrospective study; the number of participants included in the validation cohort was less than that in the training cohort, and the validation cohort included patients who were of different races and who had different distributions of pathogenesis of HCC. It is therefore possible that these differences may have influenced the results. The clinical information was also not matched between patients in the training cohort and those in the validation cohort, and therefore, we had to exclude several parameters. For example, antiviral treatment was applied in almost every patient in the training cohort, which may have affected their OS (2, 3); however, this treatment process was not recorded in the TCIA and TCGA cohorts. Nevertheless, we were able to stratify patients into two groups based on the risk of recurrence, and these findings illustrate the generalization potential of our model and provides evidence for the multicenter application of the radiomics model. Second, we set the threshold of the *P* value in the multivariable regression to 0.15 in order to develop a radiomics nomogram that incorporated all three clinical factors (i.e., AFP, tumor number, and tumor size) that were associated with a higher recurrence rate and impaired survival of patients with HCC (2, 3). After integrating both the clinical factors and radiomics features into a radiomics nomogram, the prediction accuracy surpassed that of the readily accessible clinical nomogram. Third, the VOI was manually delineated by one abdominal radiologist, and this may have led to intraobserver bias and affected the results. Secondary class verification of the delineation could ensure higher intraobserver reproducibility. Finally, we segmented the VOI in the portal venous phase (PVP) and extracted features from the single phase. The tumor boundary in the PVP may be sharper and clearer in our dataset, which is ideal for manual segmentation. In the future, we will segment the VOI in both the arterial and portal venous phases.

In conclusion, we successfully developed and validated a radiomics nomogram for the prediction of early recurrence in patients with HCC who underwent curative resection. Additionally, the predictive performance and generalizability of the radiomics nomogram, which integrated a dichotomized radiomics signature as well as clinical characteristics, were improved as compared to those of the clinical nomogram alone.

## Conflict of interest disclosure

The authors declared no conflicts of interest.

## References


1. Chen W, Zheng R, Baade PD, et al. Cancer statistics in China, 2015. CA Cancer J Clin 2016; 66:115–132. [Crossref]
2. European Association for the Study of the Liver. EASL Clinical Practice Guidelines: Management of hepatocellular carcinoma. J Hepatol 2018; 69:182–236.
3. Forner A, Reig M, Bruix J. Hepatocellular carcinoma. Lancet 2018; 391:1301–1314. [Crossref]
4. Furuta M, Ueno M, Fujimoto A, et al. Whole genome sequencing discriminates hepatocellular carcinoma with intrahepatic metastasis from multi-centric tumors. J Hepatol 2017; 66:363–373. [Crossref]
5. Tabrizian P, Jibara G, Shrager B, Schwartz M, Roayaie S. Recurrence of hepatocellular cancer after resection: patterns, treatments, and prognosis. Ann Surg 2015; 261:947–955. [Crossref]
6. Imamura H, Matsuyama Y, Tanaka E, et al. Risk factors contributing to early and late phase intrahepatic recurrence of hepatocellular carcinoma after hepatectomy. J Hepatol 2003; 38:200–207. [Crossref]
7. Portolani N, Coniglio A, Ghidoni S, et al. Early and late recurrence after liver resection for hepatocellular carcinoma: prognostic and therapeutic implications. Ann Surg 2006; 243:229–235. [Crossref]
8. Chan AWH, Zhong J, Berhane S, et al. Development of pre and post-operative models to predict early recurrence of hepatocellular carcinoma after surgical resection. J Hepatol 2018; 69:1284–1293. [Crossref]
9. Huang G, Li PP, Lau WY, et al. Antiviral therapy reduces hepatocellular carcinoma recurrence in patients with low HBV-DNA levels: a randomized controlled trial. Ann Surg 2018; 268:943–954. [Crossref]
10. Dhanasekaran R, Nault JC, Roberts LR, Zucman-Rossi J. Genomic medicine and implications for hepatocellular carcinoma prevention and therapy. Gastroenterology 2019; 156:492–509. [Crossref]
11. Dong LQ, Peng LH, Ma LJ, et al. Heterogeneous immunogenomic features and distinct escape mechanisms in multifocal hepatocellular carcinoma. J Hepatol 2020; 72:896–908. [Crossref]
12. Lambin P, Leijenaar RTH, Deist TM, et al. Radiomics: the bridge between medical imaging and personalized medicine. Nat Rev Clin Oncol 2017; 14:749–762. [Crossref]
13. Bi WL, Hosny A, Schabath MB, et al. Artificial intelligence in cancer imaging: Clinical challenges and applications. CA Cancer J Clin 2019; 69:127–157. [Crossref]
14. Aerts HJ, Velazquez ER, Leijenaar RT, et al. Decoding tumor phenotype by noninvasive imaging using a quantitative radiomics approach. Nature communications 2014; 5:4006. [Crossref]
15. Zhou Y, He L, Huang Y, et al. CT-based radiomics signature: a potential biomarker for preoperative prediction of early recurrence in hepatocellular carcinoma. Abdom Radiol (NY) 2017; 42:1695–1704. [Crossref]
16. Cozzi L, Dinapoli N, Fogliata A, et al. Radiomics based analysis to predict local control and survival in hepatocellular carcinoma patients treated with volumetric modulated arc therapy. BMC Cancer 2017; 17:829. [Crossref]
17. Kim S, Shin J, Kim DY, Choi GH, Kim MJ, Choi JY. Radiomics on gadoxetic acid-enhanced magnetic resonance imaging for prediction of postoperative early and late recurrence of single hepatocellular carcinoma. Clin Cancer Res 2019; 25:3847–3855. [Crossref]
18. Shan QY, Hu HT, Feng ST, et al. CT-based peritumoral radiomics signatures to predict early recurrence in hepatocellular carcinoma after curative tumor resection or ablation. Cancer Imaging 2019; 19:11. [Crossref]

19. Zhang Z, Jiang H, Chen J, et al. Hepatocellular carcinoma: radiomics nomogram on gadoxetic acid-enhanced MR imaging for early postoperative recurrence prediction. Cancer Imaging 2019; 19:22. [Crossref]
20. Saini A, Breen I, Pershad Y, et al. Radiogenomics and radiomics in liver cancers. Diagnostics 2018; 9:4. [Crossref]
21. Wakabayashi T, Ouhmich F, Gonzalez-Cabrera C, et al. Radiomics in hepatocellular carcinoma: a quantitative review. Hepatol Int 2019; 13:546–559. [Crossref]
22. Zheng BH, Liu LZ, Zhang ZZ, et al. Radiomics score: a potential prognostic imaging feature for postoperative survival of solitary HCC patients. BMC Cancer 2018; 18:1148. [Crossref]
23. Hui TCH, Chuah TK, Low HM, Tan CH. Predicting early recurrence of hepatocellular carcinoma with texture analysis of preoperative MRI: a radiomics study. Clin Radiol 2018; 73:1056 e11–16. [Crossref]
24. Akai H, Yasaka K, Kunimatsu A, et al. Predicting prognosis of resected hepatocellular carcinoma by radiomics analysis with random survival forest. Diagn Interv Imaging 2018; 99:643–651. [Crossref]
25. Ning P, Gao F, Hai J, et al. Application of CT radiomics in prediction of early recurrence in hepatocellular carcinoma. Abdom Radiol (NY) 2020; 45:64–72. [Crossref]
26. Yuan C, Wang Z, Gu D, et al. Prediction early recurrence of hepatocellular carcinoma eligible for curative ablation using a radiomics nomogram. Cancer Imaging 2019; 19:21. [Crossref]
27. Segal E, Sirlin CB, Ooi C, et al. Decoding global gene expression programs in liver cancer by noninvasive imaging. Nat Biotechnol 2007; 25:675–680. [Crossref]
28. Yip C, Landau D, Kozarski R, et al. Primary esophageal cancer: heterogeneity as potential prognostic biomarker in patients treated with definitive chemotherapy and radiation therapy. Radiology 2014; 270:141–148. [Crossref]
29. Liu J, Lichtenberg T, Hoadley KA, et al. An integrated TCGA Pan-cancer clinical data resource to drive high-quality survival outcome analytics. Cell 2018; 173:400–416.e11.
30. Landis JR, Koch GG. The measurement of observer agreement for categorical data. Biometrics 1977; 33:159–174. [Crossref]
31. Chou CT, Chen RC, Lin WC, Ko CJ, Chen CB, Chen YL. Prediction of microvascular invasion of hepatocellular carcinoma: preoperative CT and histopathologic correlation. AJR Am J Roentgenol 2014; 203:W253–W259. [Crossref]
32. An C, Kim DW, Park YN, Chung YE, Rhee H, Kim MJ. Single hepatocellular carcinoma: preoperative MR imaging to predict early recurrence after curative resection. Radiology 2015; 276:433–443. [Crossref]
33. Sun R, Limkin EJ, Vakalopoulou M, et al. A radiomics approach to assess tumor-infiltrating CD8 cells and response to anti-PD-1 or anti-PD-L1 immunotherapy: an imaging biomarker, retrospective multicohort study. Lancet Oncol 2018; 19:1180–1191. [Crossref]
34. Larue R, van Timmeren JE, de Jong EEC, et al. Influence of gray level discretization on radiomic feature stability for different CT scanners, tube currents and slice thicknesses: a comprehensive phantom study. Acta Oncol 2017; 56:1544–1553. [Crossref]
35. Akateh C, Black SM, Conteh L, et al. Neoadjuvant and adjuvant treatment strategies for hepatocellular carcinoma. World J Gastroenterol 2019; 25:3704–3721. [Crossref]